VNU Journal of Science: Mathematics - Physics
Journal homepage: https://js.vnu.edu.vn/MaP

Original Article

# Enhanced Resistive Switching Memory Performance of PVA-Cellulose Nanocomposites

Nguyen Hong Ngoc[1,2], Ho Phong Hoang Thinh[1,2], Tran Tuan Kiet[1,2], Tong Hoang Tuan[1,2], Pham Kim Ngoc[1,2,*]

[1]*University of Science, Vietnam National University Ho Chi Minh City, 227 Nguyen Van Cu, Cho Quan, Ho Chi Minh, Vietnam*
[2]*Vietnam National University, Vo Truong Toan, Linh Xuan, Ho Chi Minh City, Vietnam*

Received 17th April 2025
Revised 20th June 2025; Accepted 9th October 2025

**Abstract:** Flexible and sustainable materials are becoming increasingly important for next-generation electronic devices. This study examines the resistive switching behavior of a polyvinyl alcohol (PVA)–cellulose composite and its potential application in resistive switching memory. Cellulose fibers were extracted from the lotus petiole and purified with chemical agents. The composite of PVA and cellulose was used as an insulator layer in the capacitor-like structure of Ag/PVA–Cellulose/FTO. Structural analysis confirms strong interactions between PVA and cellulose, which contribute to improving material stability and film formation. Devices demonstrate reliable bipolar resistive switching at 1 V and stable endurance over 50 switching cycles. Electrical conduction mechanisms of memory devices follow the space-charge-limited current (SCLC) and Ohmic conduction at high resistance and low resistance states, respectively. This confirms the filamentary-based resistive switching mechanism within Ag/PVA–Cellulose/FTO devices. These results highlight the advantages of PVA–cellulose, offering a promising approach for developing flexible memory devices and environmentally friendly electronic materials.

*Keywords:* Cellulose fiber, PVA, Resistive switching, Analog, Space-Charge-Limited Current.

## 1. Introduction

Resistive switching memory, commonly known as resistive random-access memory (RRAM), is a non-volatile memory technology that operates by modulating the resistance across a dielectric material, effectively functioning as a memristor. This mechanism enables data storage by transitioning between

* Corresponding author.
*E-mail address:* phamkngoc@hcmus.edu.vn

https//doi.org/10.25073/2588-1124/vnumap.5001

a high-resistance state (HRS) and a low-resistance state (LRS), representing binary data. RRAM offers advantages such as high-speed operation, structural simplicity, low power consumption, scalability potential, and high-density memory storage features [1].

Memristors utilize a wide range of materials for resistive switching, including binary metal oxides such as hafnium oxide ($HfO_2$), titanium oxide ($TiO_2$), and tantalum oxide ($Ta_2O_5$), which are compatible with CMOS processing [2]. Alternative materials such as perovskite oxides, nitrides, chalcogenides, two-dimensional materials like graphene, and organic components, such as lignin, have been explored for their unique electrical properties and mechanical stability [3]. Hybrid structures combining organic and inorganic materials, such as agarose integrated with aluminum oxide ($Al_2O_3$), offer promising applications in biocompatible and biodegradable RRAM devices [4]. Cellulose-based materials have been explored in memristors due to their biodegradability, flexibility, and eco-friendliness. For instance, a study demonstrated an Al/gelatin/Ag structure on a bio-cellulose film, achieving a high ON/OFF current ratio ($>10^4$) and low operating voltage (<3 V), with the device degrading completely in soil within five days, highlighting its potential for sustainable electronics [5]. Additionally, a memory device based on a cellulose–$Ti_3C_2T_x$ MXene composite hydrogel demonstrated reliable bipolar resistive switching and multilevel switching behavior at low operating voltages (±0.5 to ±1 V), suggesting potential for low-cost, sustainable, and biocompatible memory storage applications [6]. Recent studies highlight the potential of cellulose-based materials in resistive switching memory devices, offering biodegradable and eco-friendly alternatives. A study used cellulose fibers from lotus petioles as the dielectric medium in an Ag/Cellulose/Ag/Si planar structure, demonstrating hysteresis behavior and good durability. However, the study lacked detailed insights into switching mechanisms and long-term stability under varying environmental conditions [7]. Another work focused on carboxymethyl cellulose (CMC)-graphene oxide bio-nanocomposites in Al/CMC-GO/Al/$SiO_2$ structures, showing a high ON/OFF ratio ($\sim 10^5$), low switching voltage (2.22 V), and mechanical flexibility. Despite these advantages, the long-term thermal stability and compatibility with large-scale fabrication were not fully addressed [8]. Additionally, a study demonstrated a fully biodegradable resistive memory device using an Al/gelatin/Ag structure on a bio-cellulose (BC) substrate, achieving a high ON/OFF ratio ($>10^4$) and full degradation in soil within five days. However, the potential degradation of performance in humid conditions and real-world applications remains a challenge [5]. Collectively, these studies emphasize the promise of cellulose-based materials in sustainable memory devices while highlighting the need for improved stability, scalability, and environmental resilience.

The integration of cellulose and polyvinyl alcohol (PVA) holds significant promise for applications in memristors, owing to their complementary properties. Cellulose, a natural polymer, offers excellent mechanical strength, thermal stability, and biodegradability, while PVA is known for its film-forming ability, flexibility, and high dielectric strength. These attributes suggest that a cellulose-PVA composite could serve as an effective dielectric material in RRAM architectures. Several studies have explored the electrical properties of cellulose-PVA blends, providing a foundation for their potential use in memory devices. For instance, research on carboxymethyl cellulose (CMC) and PVA-based biopolymer blend electrolytes demonstrated ionic conductivities reaching up to $9.12 \times 10^{-6}$ S/cm at room temperature, indicating favorable electrical characteristics for such composites. [9]. Additionally, studies on the dielectric properties and AC conductivity of cellulose-PVA blends have shown promising results, further supporting their suitability for electronic applications. [10]. Moreover, the development of flexible memristors using PVA-graphene oxide (GO) hybrid nanocomposites has been reported, exhibiting excellent electrical performance at ultralow voltages below 0.5 V and high stability under mechanical stress. These devices also demonstrated low power consumption during the SET process and mimicked Pavlovian-associative learning behaviors, highlighting Their potential for neuromorphic computing applications [11]. Given these findings, further research is warranted to optimize the

cellulose-PVA composite system for RRAM applications. Investigations focus on enhancing the electrical conductivity and dielectric properties of the composites and ensuring the material's stability and reliability under operational conditions.

In this study, we integrated cellulose from lotus fibers with PVA and utilized this composite as a switching medium in memory devices. The microstructure, surface morphology, and resistive switching characteristics of Ag/PVA-Cellulose/FTO have been investigated thoroughly. The results found that the composite-based device significantly enhances the endurance compared to pure devices. It suggests that the composite-based device may be applied in data storage, neuromorphic synapses, and bioelectronics.

## 2. Materials and Methods

### *2.1. Materials*

The lotus petioles were collected from the Ho Thi Ky market, Ho Chi Minh City. Chemicals including sodium hypochlorite (NaClO), sulfuric acid ($H_2SO_4$), sodium hydroxide (NaOH), purity ≥ 99.8%, acetone ($C_3H_6O$, 99.5%), ethanol ($C_2H_6O$, 99.5%), polyvinyl alcohol (PVA, Mw = 89,000 – 98,000, 99%) and silver target (Ag, 3’ dia, purity 99.99%) were purchased from Sigma.

### *2.2. Preparation of Cellulose Fibers*

Cellulose was isolated through acid hydrolysis to remove lignin, wax, oil, and hemicellulose from lotus silk. The raw silk was manually extracted from white lotus petioles by making a small incision, uncoiling the fibers, and cutting them into ~2.0 cm segments. The fibers were subjected to ultrasonic treatment in DI water and ethanol for 1 hour, followed by washing and soaking in 8% NaClO until a neutral pH was achieved. Subsequently, the fibers underwent hydrolysis with 98% $H_2SO_4$ for 1 hour, followed by centrifugation at 3000 rpm. They were then treated with NaOH for 2 hours and washed to remove residual impurities. The final cellulose was oven-dried at 70 °C until a constant mass was achieved and stored for further analysis. All reagents used were of analytical grade and required no additional purification.

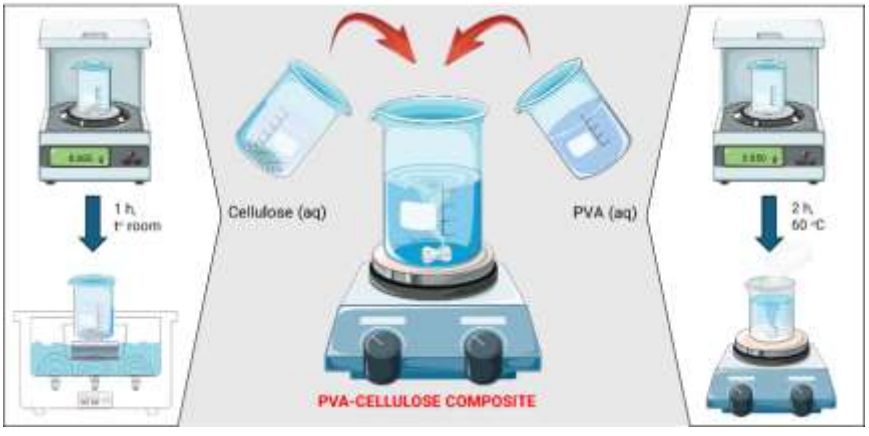


Figure 1. Synthesis process of PVA-Cellulose composite.

### *2.3. Fabrication of Ag/PVA-Cellulose/ITO RRAM Device*

The PVA-cellulose composite was prepared in advance for device fabrication. Cellulose powder was dispersed in DI water using ultrasonication for 1 hour at room temperature. Simultaneously, PVA was dissolved in DI water at a mass ratio of 10:1 (PVA:Cellulose) and stirred magnetically at 60 °C for 2 hours. The cellulose dispersion was then heated to 60 °C and the PVA solution was slowly added dropwise under continuous magnetic stirring to ensure uniform dispersion. Upon completing the addition, the mixture was stirred further at 60 °C for 2 hours (Figure 1).

Commercial fluorine-doped tin oxide (FTO) substrates, measuring 1×1 cm², were sequentially cleaned using acetone, DI water, and ethanol to remove surface contaminants. Following the cleaning process, the substrates were carefully dried to prevent any damage to the conductive surface. A heat-resistant electronic adhesive (~0.2 cm wide) was applied to the substrate surface to create a connection point for the bottom electrode during current-voltage characterization. Next, 20 µL of the dispersed PVA-cellulose composite was dropped onto the FTO substrate by the spin-coating method. In each drop, the substrate was heated at 60°C for 15 minutes to evaporate the solvent. After the last drop, the sample was incubated at 60°C for 30 minutes to ensure the complete removal of any remaining solvent from the membrane structure. Finally, once the PVA-cellulose membrane was successfully formed on the FTO substrate, the top electrode was fabricated using silver (Ag) via DC magnetron sputtering. An aluminum mask with circular holes (1 mm in diameter) was used to shape and define the electrode area. The fabrication approach for a device with a three-layer structure: Ag/PVA-Cellulose/FTO RRAM is described in Figure 2.

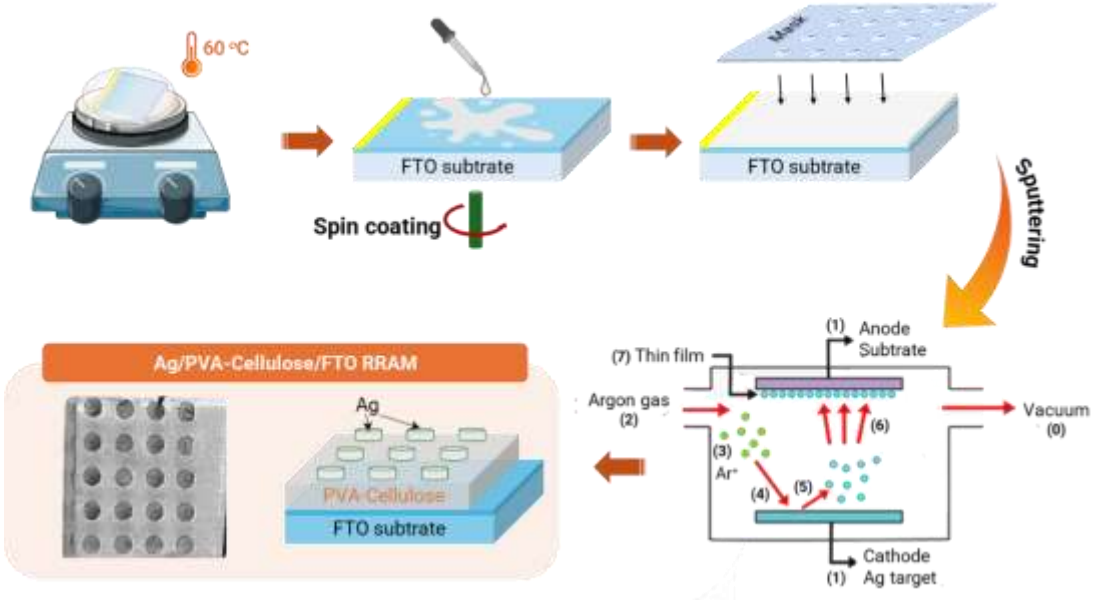


Figure 2. Process of fabrication Ag/PVA-Cellulose/FTO RRAM.

*2.4. Sample Characterization*

The structural properties of PVA-cellulose films were analyzed using powder X-ray diffraction (D8 Diffractometer, Bruker, 40 kV, and 30 mA), employing nickel-filtered Cu Kα radiation. Fourier transform infrared spectroscopy (TENSOR 27, Bruker, Germany) to investigate the chemical bonds and functional groups. All measurements were performed in step-scan mode at ambient temperature. The surface morphology and cross-sectional thickness of the films were examined using a scanning electron

microscope (SEM; Hitachi S4800) operating at an accelerating voltage of 10 kV. Electrical measurements were carried out with a Keithley 4200-SCS parameter analyzer, using a single source measurement unit (SMU) to apply voltage to the Ag upper electrode. The lower electrode was grounded via the analyzer's ground unit.

## 3. Results and Discussion

### *3.1. Structural Results of Cellulose, PVA and Composite*

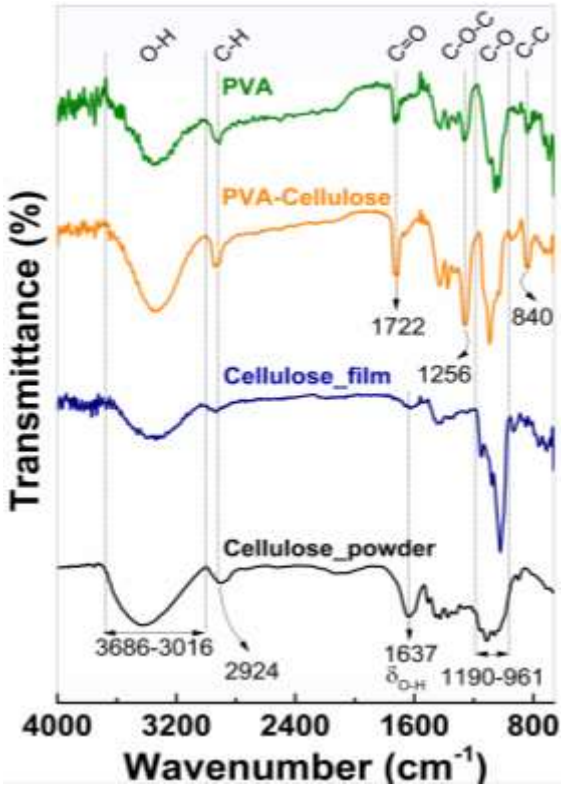


Figure 3. FTIR spectra of Cellulose, PVA, and PVA-cellulose composite.

Figure 3 illustrates the FT-IR spectra of cellulose, PVA, and PVA-Cellulose composite materials. The spectrum of cellulose reveals characteristic absorption bands of an organic polysaccharide, including peaks at 1631, 1061, and 557 $cm^{-1}$, corresponding to O-H bending, C-OH stretching, and bending vibrations, respectively. These cellulose-specific peaks overlap with functional groups of PVA, indicating molecular interactions between PVA and cellulose.

The pure PVA spectrum displays a broad absorption band at 3441 $cm^{-1}$, attributed to O-H stretching vibrations, a signal of hydrogen bonding in PVA. In the PVA-cellulose, this hydroxyl peak at 3428 $cm^{-1}$ is broader and blue-shifted. This shift suggests a disruption of intra- and intermolecular hydrogen bonds within cellulose due to its interaction with the PVA matrix. Other features of the PVA spectrum include a band at 2924 $cm^{-1}$, corresponding to CH and $CH_2$ asymmetric stretching vibrations. A medium-intensity peak at 1722 $cm^{-1}$ represents the C=O stretching vibration of ester and carboxyl groups formed during PVA polymerization. These peaks exhibit the same tendency toward increased intensity in the

composite, reflecting the incorporation of cellulose and the thermal treatment applied during film formation. The peak at 1256 $cm^{-1}$, observed in both PVA and PVA-cellulose spectra, is associated with $CH_2$ stretching and C–O–C vibrations. Additionally, a strong band at 1061 $cm^{-1}$ is identified as the C-O stretching mode of PVA, which decreases in the PVA-Cellulose film due to the defects of cellulose. Furthermore, the peak observed at 851 $cm^{-1}$ in the pure PVA is attributed to the C-C stretching vibration, and its intensity increases in the composite, further indicating enhanced interactions between cellulose and PVA.

*3.2. Morphological Surface of Cellulose, PVA and Composite*

The SEM images of cellulose fibers at two different magnifications reveal a smooth surface, with fiber diameters ranging from 3.4 to 4.6 µm, as shown in Figure 4 (a1, a2). The fibers are long, interwoven, and randomly distributed across the sample surface, with nearly no detectable impurities. In contrast, the PVA micrographs exhibit a homogeneous, smooth, and featureless surface morphology, characteristic of their amorphous nature and film-forming ability (Figure 4 (b1, b2)). This structural uniformity reflects the flexibility and hydrophilic properties of PVA, which enhance its compatibility with other materials.

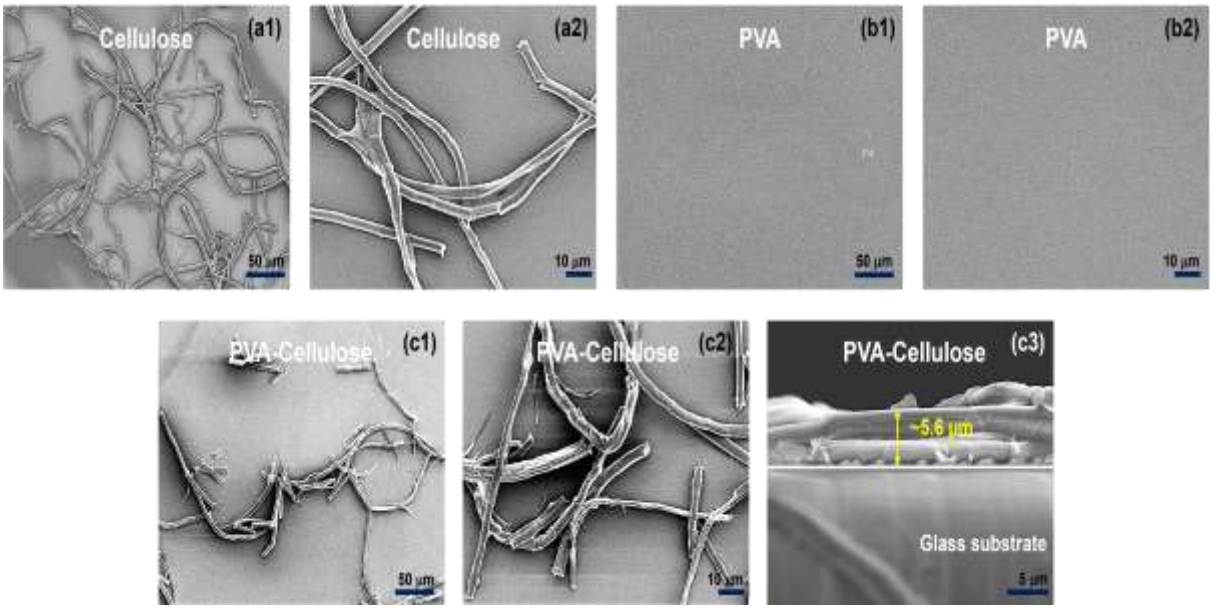


Figure 4. SEM images of (a1, a2) Surface Cellulose, (b1, b2) PVA, (c1,c2) their compounds at different magnifications, and (c3) cross-section.

Upon incorporating cellulose into the PVA matrix, no significant changes are observed in the morphology or fiber diameter of the cellulose fiber network revealed in Figure 4 (c1, c2). The PVA-cellulose film consists of cellulose fibers embedded within the polymer, with an approximate thickness of 5.6 µm, enhancing the composite's mechanical and flexible properties, as seen in Figure 4 (c3). These morphological observations highlight the synergistic behavior of the cellulose-PVA composite, which suggests suitability for sustainable films and functional membranes.

*3.3. Resistive Switching Characteristics of Cellulose, PVA and Composite Based Devices*

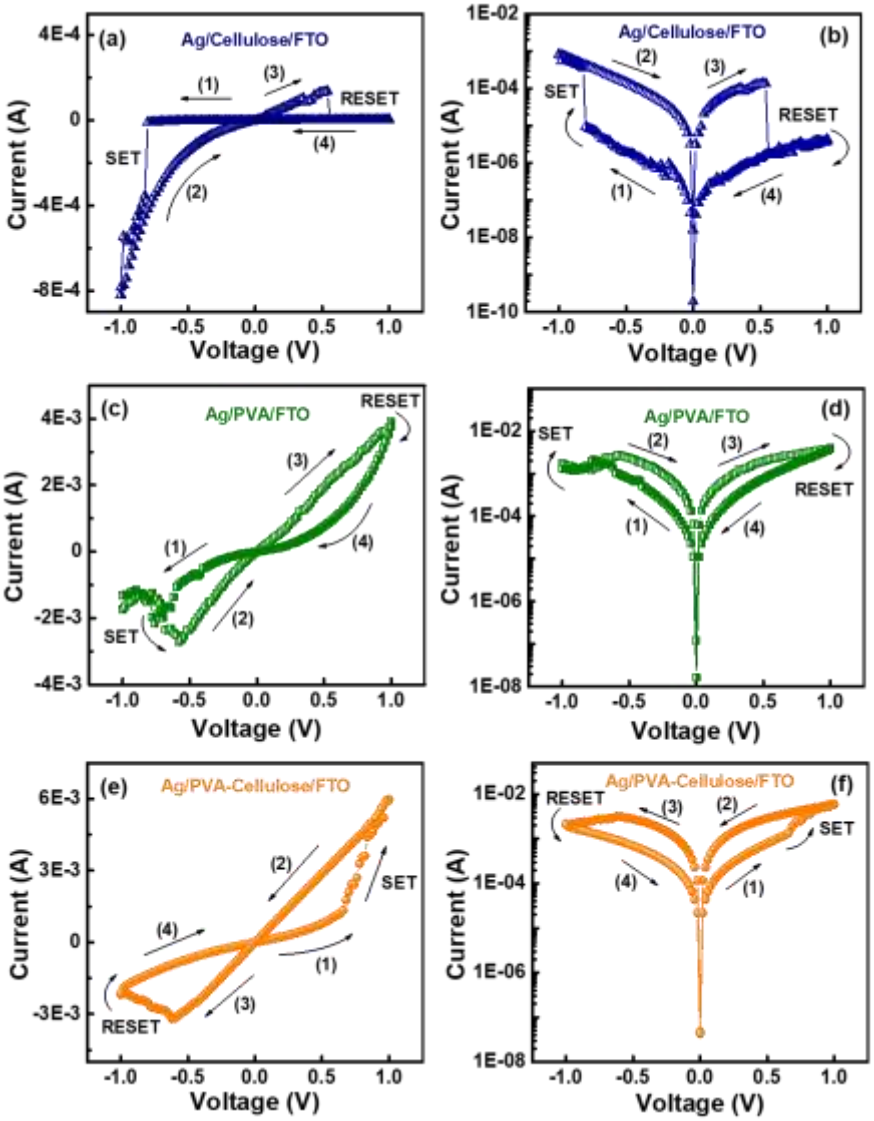


Figure 5. Linear and semi-logarithmic I-V characteristics of the Ag/PVA-Cellulose/FTO.

The resistive switching (RS) behavior of cellulose, polyvinyl alcohol (PVA), and PVA–cellulose composite devices is examined through their I-V characteristics under the sweeping mode. The fabricated devices initially exhibit readout currents in the microampere range, indicating a stable insulating state. The I-V characteristics of the devices demonstrate reversible RS behavior, operating at low voltages within the range of −1.0 V to 1.0 V. For the Ag/Cellulose/FTO shown in Figure 5(a, b), the current gradually increase when the voltage sweeps from 0 to -1 V. At the threshold voltage, the device transits from the insulating state (OFF) to the conductive state (ON), marking the SET operation. When the external bias reached -1 V, the hysteresis window expands, and the current abruptly increases to approximately $5\times10^{-4}$ A around the threshold voltage $V_{SET}$ ~ -0.8 V. This transition corresponds to the switching from the high-resistance state (HRS) to the low-resistance state (LRS), referred to as the

"write" process. As the voltage is reduced from −1.0 V to 0 V, the conduction current gradually decreases, returning to ~ $10^{-6}$ A. The "erase" process corresponds to the transition from LRS → HRS. When the voltage is swept from 0 V to 1.0 V and back to 0 V, the reset behavior is observed under positive bias. The resulting I-V characteristics confirm the non-volatility of the memory device.

Similarly, the PVA-based device also exhibits analog-like RS behavior within the voltage range of -1.0 V to +1.0 V (Figure 5(c, d)). During voltage sweeping from 0 V to -1.0 V, the device current increases from ~ $10^{-4}$ A to ~ $10^{-3}$ A before decreasing as the voltage approaches its maximum value (RESET process). The current then decreases gradually in a voltage-dependent manner.

In contrast to the previous two samples, the PVA–cellulose–based device exhibits non-volatile bipolar RS behavior (Figure 5(e, f)). In the first stage, as the voltage increases from 0 V to 1.0 V, the current gradually increases from ~ $10^{-4}$ A to ~$5\times10^{-3}$ A at $V_{SET}$ = 0.65 V, indicating the transition from HRS to LRS (SET process). The current then remains in LRS until the RESET process is initiated during the negative voltage sweep from 0 V to -1.0 V. The RESET voltage occurs at -0.98 V, where the current decreases from ~ $5\times10^{-3}$ A to ~ $10^{-4}$ A.

### *3.4. Endurance of the Composite-base Device*

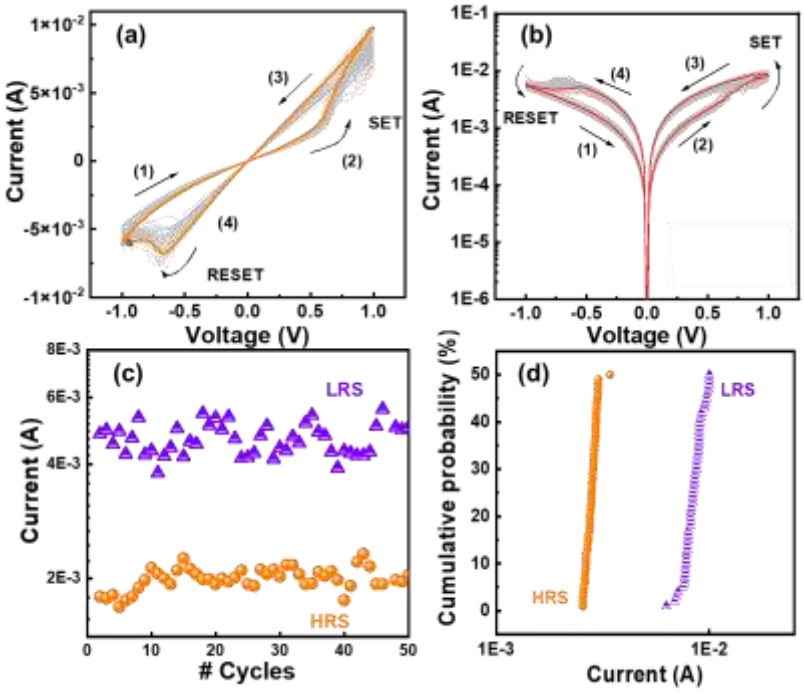


Figure 6. (a) The linear and (b) semi-logarithmic plot of I–V endurance characteristics of the Ag/PVA-Cellulose/FTO device, (c and d) the distribution of current at HRS and LRS during 50 cycles.

The pure cellulose and pure PVA-based devices exhibit low endurance with several cycling sweeps. On the other hand, the PVA-cellulose devices show high endurance characteristics for multiple switching cycles. The endurance and current distribution results of HRS and LRS of the Ag/PVA–Cellulose/ITO are presented in Figure 6. The I-V characteristics in linear and semi-log plots remain reproducible over 50 consecutive ON/OFF cycles in the low operating voltage of 1 V (Figure 6a-b). Furthermore, the statistical distribution for Ag/PVA–Cellulose/FTO exhibits relative stability in both

HRS and LRS states, with currents in the range of $10^{-3}$ - $10^{-2}$ A (Figure 6c). The LRS current (represented by purple triangles) and HRS current (orange circles) remain well-separated, ensuring distinct memory states. The current at LRS has more fluctuation than it does at HRS. This variation can be from the random charge transfers via the conducting channels under an electric field. The cumulative probability plot (Figure 6d) further emphasizes the consistency of resistance states, with clear differentiation between LRS and HRS, indicating a strong potential for non-volatile memory applications.

### *3.5. Device-to-Device Repeatability*

Figure 7 (a–h) shows the I–V characteristics of four individual devices with an Ag/cellulose-PVA/FTO structure. The top row presents the plot in linear scale (a-d), while the bottom row shows the same curves in semi-logarithmic scale (e-h) to highlight currents in both high and low resistance states. All devices exhibit clear and consistent bipolar switching behavior, with distinguishable SET in the positive bias and RESET in the negative bias. While minor variations in current amplitude or switching sharpness can be observed, the overall tendencies and switching voltages are comparable across devices. This suggests that the fabrication process yields reliable and repeatable device performance. The good agreement between devices confirms the stability of the cellulose-based switching layer and its suitability for memory applications requiring uniform behavior across multiple cells. These results may imply that the resistive switching mechanism is not strongly affected by local variations in the cellulose structure or electrode contact.

The charge transport characteristics of the Ag/Cellulose/FTO, Ag/PVA/FTO, and Ag/PVA–Cellulose/FTO devices reveal fundamentally distinct conduction mechanisms under applied electric fields, governed by trap states, polymer structure, and interfacial effects.

For the Ag/Cellulose/FTO structure, the forward voltage sweep from 0 to -1 V exhibits three regimes. At low electric fields, the current follows a near-linear conduction ($S \approx 1.5$), indicative of Ohmic or shallow trap-assisted transport. As the field increases, the slope rises to ~2, following a space-charge-limited current (SCLC) regime where injected carriers begin to occupy trap states. At even higher electric field ($S \approx 3.1$), a trap-filled limit (TFL) behavior emerges, consistent with deep trap saturation and the formation of conductive filaments, marking the transition to the low resistance state. These features above align with classical SCLC theory in disordered dielectrics [12], [13]. During the reverse sweep, the current remains high, with $S \approx 2.7$ at strong fields, gradually returning to Ohmic behavior as the field approaches zero. This persistence supports a stable, non-volatile conduction pathway, likely governed by filamentary or interface-stabilized transport.

The Ag/PVA/FTO device, though initially thought to exhibit purely Ohmic conduction, shows nonlinearity upon closer observation. In the forward sweep, a slope of $S \approx 1.1$ suggests drift-dominated transport with slight field-dependent mobility. In the reverse sweep, the slope increases to $S \approx 1.5$, implying weak trap-assisted conduction or minor field-induced polarization effects within the PVA matrix. The asymmetry and mild nonlinearity point to the presence of shallow traps or interfacial dipole interactions. Notably, the slight degradation at the high electric field may relate to the complex mechanism. This behavior is consistent with reports on pristine PVA films, where local structural disorder or residual ionic motion contributes to deviations from ideal Ohmic conduction [14], [15].

In comparison, the Ag/PVA–Cellulose/FTO structure exhibits a hybrid behavior that blends the switching functionality of cellulose with the stabilizing effects of PVA. During the forward sweep, the current increases nonlinearly, with $S \approx 2$ at intermediate fields and $S \approx 3.3$ at higher fields, characteristic of SCLC and TFL regimes. Remarkably, the reverse sweep is fully Ohmic ($S \approx 1$) across the entire bias range, indicating the formation of a uniform and stable conductive path. The improved electrical homogeneity is likely a result of the PVA component mitigating structural and energetic disorder in the active layer.

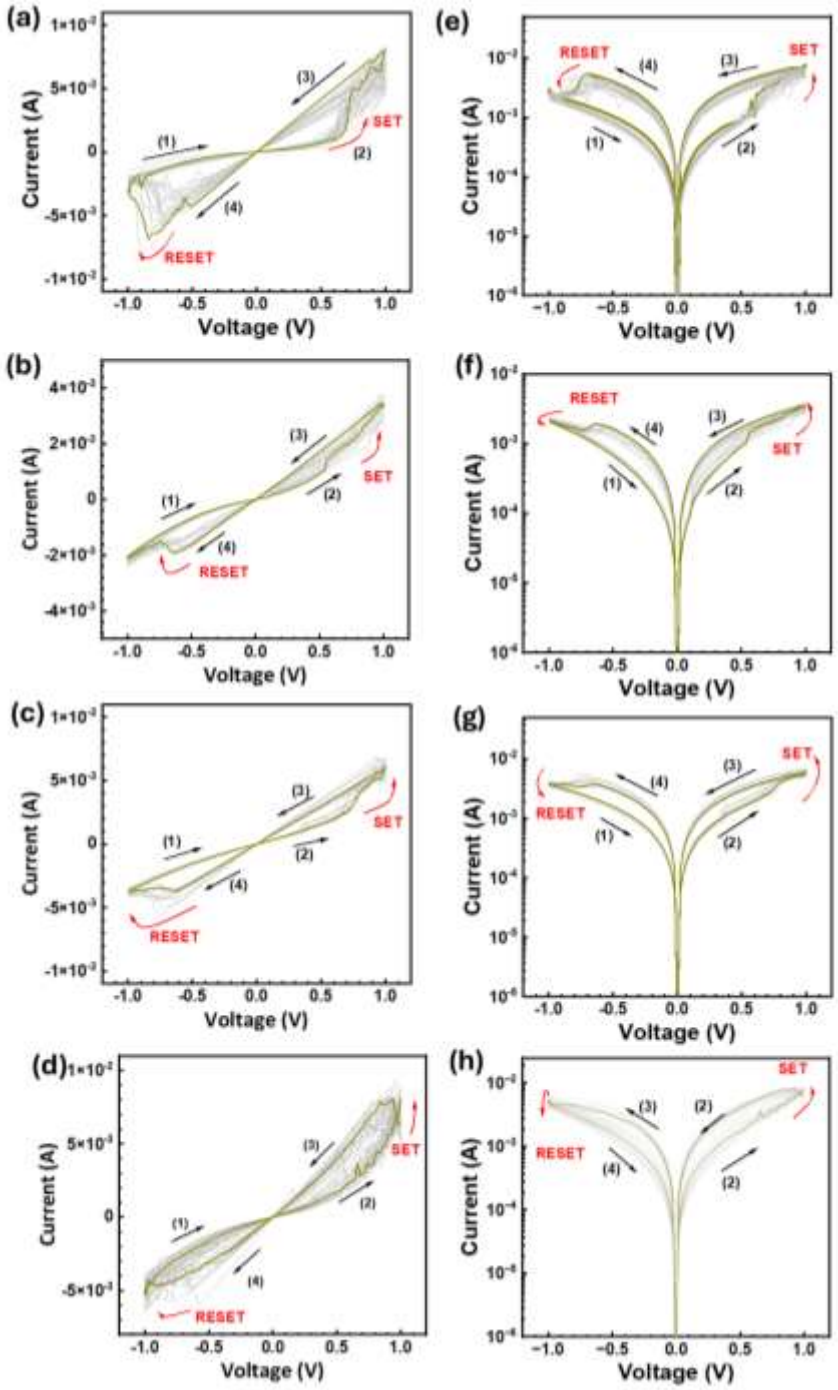


Figure 7. The linear (a-d) and semi-logarithmic (d-h) I-V plots of memory devices.

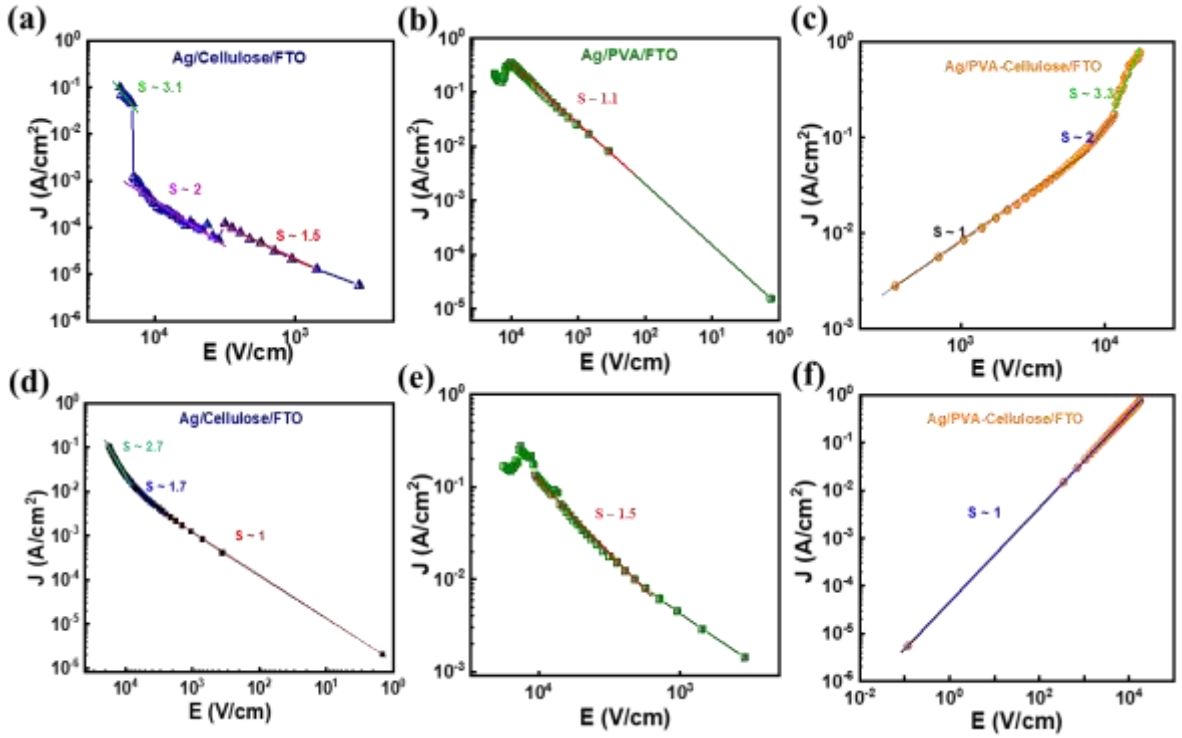


Figure 8. Electrical conduction mechanisms of cellulose-based devices. The J-E plots of the first and second stages of Ag/Cellulose/FTO (a, d), Ag/PVA/FTO (b, e), and Ag/PVA–Cellulose/FTO (c, f).

## Conclusions

This study highlights the enhancement of the PVA–cellulose composite-based device compared to the pure cellulose-based device, particularly in improving the resistive switching behavior. FTIR spectra confirm strong interactions between PVA and cellulose, which lead to structural integration and material stability. SEM images show that while cellulose fibers still keep their structure, embedding them in the PVA matrix may enhance flexibility and film formation. Current-voltage measurements reveal that the device exhibits bipolar resistive switching, reliable and repeatable from device to device. The electrical conduction analysis highlights the cellulose's enables trap-mediated switching behavior, PVA's contribution of conduction stability and retention. Their combination in a hybrid matrix presents an effective strategy for resistive memory devices that balances performance and reliability. These findings suggest that cellulose-PVA composite is a strong candidate for use in flexible electronics, biocomposites, and memory devices.

## Author's contribution

Nguyen Hong Ngoc: Methodology, Writing - original draft, Ho Phong Hoang Thinh, Tran Tuan Kiet: Data Curation and Investigation, Tong Hoang Tuan: Formal analysis, and Pham Kim Ngoc: Conceptualization, Supervision, Writing – review & editing.

## Competing Interests

The authors declare that they have no competing interests.

## Acknowledgments

This research is funded by Vietnam National Foundation for Science and Technology Development (NAFOSTED) under grant number 103.02-2021.86.

## Availability of Data and Materials

Data and materials used and/or analyzed during the current study are available from the corresponding author on reasonable request.

## References

[1] G. U. Kamble, A. P. Patil, R. K. Kamat, J. H. Kim, T. D. Dongale, Promising Materials and Synthesis Methods for Resistive Switching Memory Devices: A Status Review, ACS Appl Electron Mater, Vol. 5, No. 5, 2023, pp. 2454–2481, https//doi.org/10.1021/acsaelm.3c00062.

[2] F. Zahoor, T. Z. Azni Zulkifli, F. A. Khanday, Resistive Random Access Memory (RRAM): an Overview of Materials, Switching Mechanism, Performance, Multilevel Cell (mlc) Storage, Modeling, and Applications, Nanoscale Res Lett, Vol. 15, No. 1, 2020, pp. 90, https//doi.org/10.1186/s11671-020-03299-9.

[3] F. Zahoor et al., Resistive Random Access Memory: Introduction to Device Mechanism, Materials and Application to Neuromorphic Computing, Discover Nano, Vol. 18, No. 1, 2023, pp. 36, https//doi.org/10.1186/s11671-023-03775-y.

[4] T. H. V. Nguyen et al., Bioresorbable Resistive Switching Device Based on Organic/Inorganic Hybrid Structure for Transient Memory Applications, Adv Electron Mater, Vol. 10, No. 5, 2024, https//doi.org/10.1002/aelm.202300759.

[5] W. Y. Huang, Y. C. Chang, Y. F. Sie, C. R. Yu, C. Y. Wu, Y. L. Hsu, Bio-Cellulose Substrate for Fabricating Fully Biodegradable Resistive Random Access Devices, ACS Appl Polym Mater, Vol. 3, No. 9, 2021, pp. 4478–4484, https//doi.org/10.1021/acsapm.1c00485.

[6] T. R. Desai, S. S. Kundale, T. D. Dongale, C. Gurnani, Evaluation of Cellulose–MXene Composite Hydrogel Based Bio-Resistive Random Access Memory Material as Mimics for Biological Synapses, ACS Appl Bio Mater, Vol. 6, No. 5, 2023, pp. 1763-1773, https//doi.org/10.1021/acsabm.2c01073.

[7] H. H. Do Ho et al., Development of Switching Memory Devices of Cellulose Fibers From Lotus Petioles, Journal of Materials Science: Materials in Electronics, Vol. 35, No. 6, 2024, pp. 387, https//doi.org/10.1007/s10854-024-12134-1.

[8] T. Liu et al., Fabrication of Carboxymethyl Cellulose and Graphene Oxide Bio-Nanocomposites for Flexible Nonvolatile Resistive Switching Memory Devices, Carbohydr Polym, Vol. 214, 2019, pp. 213-220, https//doi.org/10.1016/j.carbpol.2019.03.040.

[9] M. A. Saadiah, A. S. Samsudin, Electrical Study on Carboxymethyl Cellulose-Polyvinyl Alcohol Based Bio-Polymer Blend Electrolytes, IOP Conf Ser Mater Sci Eng, Vol. 342, 2018, pp. 012045, https//doi.org/10.1088/1757-899X/342/1/012045.

[10] A. H. Salama, M. Dawy, A. M. A. Nada, Studies on Dielectric Properties and AC-Conductivity of Cellulose Polyvinyl Alcohol Blends, Polym Plast Technol Eng, Vol. 43, No. 4, 2004, pp. 1067–1083, https//doi.org/10.1081/PPT-200030024.

[11] W. Xiong et al., Flexible Poly(Vinyl Alcohol)–Graphene Oxide Hybrid Nanocomposite Based Cognitive Memristor with Pavlovian-Conditioned Reflex Activities, Adv Electron Mater, Vol. 6, No. 5, 2020, https//doi.org/10.1002/aelm.201901402.

[12] M. Sajedi Alvar, P. W. M. Blom, G. J. A. H. Wetzelaer, Space-charge-limited Electron and Hole Currents in Hybrid Organic-Inorganic Perovskites, Nat Commun, Vol. 11, No. 1, 2020, pp. 4023, https//doi.org/10.1038/s41467-020-17868-0.

[13] G. Cucinotta et al., Space Charge-Limited Current Transport Mechanism in Crossbar Junction Embedding Molecular Spin Crossovers, ACS Appl Mater Interfaces, Vol. 12, No. 28, 2020, pp. 31696-31705, https//doi.org/10.1021/acsami.0c07445.

[14] K. Uto et al., Humidity-Responsive Polyvinyl Alcohol/Microcrystalline Cellulose Composites with Shape Memory Features for Hair-Styling Applications, Adv Mater Interfaces, Vol. 11, No. 1, 2024, pp. 2300274, https://doi.org/10.1002/admi.202300274.

[15] Y. Wang, L. Zhang, A. Lu, Highly Stretchable, Transparent Cellulose/Pva Composite Hydrogel for Multiple Sensing and Triboelectric Nanogenerators, J. Mater. Chem. A, Vol. 8, No. 28, 2020, pp. 13935-13941, https//doi.org/10.1039/D0TA02010A.